Excitons in tubular molecular aggregates

Didraga, C; Knoester, J

Published in:
Journal of Luminescence

DOI:
10.1016/j.jlumin.2004.08.015

Publication date:
2004

Available online at www.sciencedirect.com
SCIENCE DIRECT®
Journal of Luminescence 110 (2004) 239–245
JOURNAL OF LUMINESCENCE
www.elsevier.com/locate/jlumin

Excitons in tubular molecular aggregates

Cătălin Didraga, Jasper Knoester*

Institute for Theoretical Physics and Materials Science Center, University of Groningen, Nijenborgh 4, 9747 AG Groningen, The Netherlands

Received 19 July 2004
Available online 22 September 2004

Abstract

We present a brief overview of recent work on the optical properties of molecular aggregates with a tubular (cylindrical) shape. The exciton states responsible for these properties can be distinguished with regard to a transverse wave number, which directly relates to optical selection rules and polarization direction of the associated absorption line. We discuss two types of analytical solutions for the exciton wave functions and the associated absorption and dichroism spectra.

PACS: 71.35.Aa; 71.35.Cc; 78.67.−n; 33.55.Ad

Keywords: Light harvesting; Dichroism

1. Introduction

Recently, molecular aggregates with a tubular geometry have attracted growing attention. Cylindrical aggregates consisting of thousands of bacteriochlorphyll molecules exist as natural light-harvesting systems in the chlorosomes of green bacteria. For Chloroflexus aurantiacus, these cylinders have a diameter of ~5 nm and a length up to hundreds of nanometer [1,2]. Interestingly, recently a class of carbocyanine dye molecules (amphiphilic substituents of the dye 5,5′,6,6′-tetrachlorobenzimidacarbocyanine) has been synthesized that self-assemble into tubular aggregates as well, with typical diameters of 10 nm [3,4]. The precise morphology of these tubes can be altered by varying side groups and solvent, leading to the perspective of preparing in a controlled way a variety of energy transport nanowires. The optical properties and dynamics of cylindrical molecular aggregates are governed by Frenkel excitons. If the effects of disorder may be ignored, the cylindrical symmetry leads to interesting optical selection rules for these states. In

*Corresponding author. Tel.: +31-50-363-4369; fax: +31-50-363-4947.
E-mail address: knoester@phys.rug.nl (J. Knoester).

0022-2313/$ - see front matter © 2004 Elsevier B.V. All rights reserved.
doi:10.1016/j.jlumin.2004.08.015

particular, only a few superradiant exciton transitions occur, which either are polarized parallel or perpendicular to the cylinder axis [5–7].

In this paper, we address several recent developments regarding these types of aggregates. In particular we address the model (Section 2), the nature of the exciton states (Section 3), and the resulting spectra, including the comparison between theory and experiment (Section 4). We conclude in Section 5.

2. Model and separation of transverse exciton momenta

The general geometry of a cylindrical molecular aggregate may be generated by rolling a two-dimensional lattice onto a cylinder surface such that the structure has the proper periodicity in the circumferential direction. Assuming that each unit cell is occupied by one molecule, it then follows [6] that the general aggregate structure may be viewed as an equidistant stack of N_1 rings (labeled $n_1 = 1, \ldots, N_1$), each containing N_2 equidistant molecules (labeled $n_2 = 1, \ldots, N_2$; Fig. 1). Each ring has radius R; adjacent rings are separated by a distance h and are rotated relative to each other over a "helical" angle γ ($0 \leqslant \gamma < 2\pi/N_2$). Connecting the closest molecules on neighboring rings, we see that the structure may also be viewed as a collection of N_2 helices winding around the cylinder (dashed line in Fig. 1). In our labeling of the molecules, we will use the convention that $n_2 =$ const. refers to a set of molecules on one such helix; $n_1 =$ const. refers to the molecules on one ring.

We will assume that each molecule has one dominant optical transition, with a transition dipole that is equal in magnitude (μ) and orientation with respect to the local frame of the cylinder. In particular, every dipole makes an angle β with the z-axis (the axis of the cylinder), while its projection on the xy plane makes an angle α with the local tangent to the ring on which the molecule resides.

The electronically excited states of the system are described by a Frenkel exciton Hamiltonian.

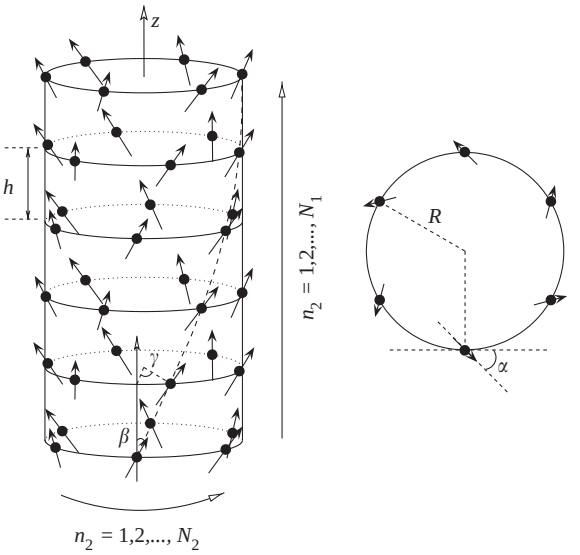

Fig. 1. Cylindrical aggregate consisting of a stack of N_1 rings that each contain N_2 molecules. The arrows indicate the transition dipoles, which are equal in magnitude (μ) and make an angle β with the cylinder axis. The projection of each dipole on the plane of the rings makes an angle α with the local tangent to the ring. Each ring is rotated with respect to the previous one over an angle γ, so that we may view the aggregate as a collection of N_2 parallel helices (dashed) on the cylinder's surface. The projection of one ring on a plane perpendicular to the cylinder's axis is shown to the right.

Setting $\hbar = 1$, we have

$$H = \omega_0 \sum_{\mathbf{n}} b_{\mathbf{n}}^{\dagger} b_{\mathbf{n}} + \sum_{\mathbf{n},\mathbf{m}}{}' J(\mathbf{n}-\mathbf{m}) b_{\mathbf{n}}^{\dagger} b_{\mathbf{m}}, \tag{1}$$

where $b_{\mathbf{n}}^{\dagger}$ and $b_{\mathbf{n}}$ denote the Pauli operators for creation and annihilation of an excitation on molecule $\mathbf{n}$, respectively, as they were first introduced by Agranovich [8]. Furthermore, ω_0 is the molecular transition frequency and $J(\mathbf{n}-\mathbf{m})$ is the excitation transfer interaction between molecules $\mathbf{n}$ and $\mathbf{m}$, which is derived from the interaction between the transition dipoles of both molecules. Due to the symmetry of the system the interaction only depends on the relative positions of the two molecules. The prime on the summation indicates that the term with $\mathbf{n} = \mathbf{m}$ is excluded.

The one-exciton eigenstates of the Hamiltonian determine the linear optical properties (absorption, linear and circular dichroism) of the aggregate. Generally these states follow from an

$N_1N_2 \times N_1N_2$ matrix diagonalization. However, the situation is simplified as a result of the cylindrical symmetry, which dictates a Bloch form for the excitons in the circumferential direction. Explicitly we may write the exciton states as

$$|\mathbf{k}\rangle = |(k_1,k_2)\rangle = \frac{1}{\sqrt{N_2}} \sum_{\mathbf{n}} e^{i2\pi k_2 n_2/N_2} \times \varphi_{k_1}(n_1;k_2) b_{\mathbf{n}}^{\dagger}|g\rangle, \quad (2)$$

with energy $E_{\mathbf{k}} = E_{(k_1,k_2)}$. Here $|g\rangle$ is the overall ground state (with all molecules in their ground state), k_2 is the transverse momentum of the wave function, taking the values $k_2 = 0, \pm1, \pm2, \ldots, \pm(N_2/2-1), N_2/2$ for N_2 even ($k_2 = 0, \pm1, \pm2, \ldots, \pm(N_2-1)/2$ for N_2 odd), and k_1 labels the longitudinal eigenfunctions $\varphi_{k_1}(n_1;k_2)$. These are eigenfunctions (with energy $E_{\mathbf{k}}$) of the effective one-dimensional exciton Hamiltonian with "molecular" frequencies $\omega_0 + \sum'_{n_2} J(n_1=0,n_2)e^{-i2\pi k_2 n_2/N_2}$ and effective "intermolecular" interaction [6]

$$J(n_1;k_2) = \sum_{n_2}{}' J(n_1,n_2) e^{-i2\pi k_2 n_2/N_2}. \quad (3)$$

The physical meaning of $J(n_1;k_2)$ is the total transfer interaction between all molecules of two rings that are separated by $n_1 h$ and that both reside in their Bloch state with momentum k_2. The overall inversion symmetry of the cylinder's Hamiltonian guarantees that each eigenenergy is at least doubly degenerate (unless $k_2 = 0$ or $k_2 = N_2/2$). More explicitly, the set of eigenstates of transverse wave number k_2 is degenerated with those of wave number $-k_2$, and the associated longitudinal eigenfunctions are each other's complex conjugates [6].

The linear optical spectra only involve the bands with $k_2 = 0$ and $k_2 = \pm1$ (degenerate) [6]. Hence, calculating those spectra involves the diagonalization of two $N_1 \times N_1$ problems, instead of one $N_1N_2 \times N_1N_2$ diagonalization.

3. Analytical expressions for the longitudinal eigenfunctions

It is of interest to have analytical solutions for the longitudinal exciton wave functions, $\varphi_{k_1}(n_1;k_2)$, obtained from diagonalizing the one-dimensional exciton problem with effective interactions $J(n_1;k_2)$ defined in Eq. (3). These are long-range interactions and, owing to the helical nature of the cylinder, they are complex (unless $k_2 = 0$) [6]. Obviously, analytical solutions may be obtained by imposing periodic boundary conditions along the cylinder's axis direction. This yields Bloch states as solutions: $\varphi_{k_1}(n_1;k_2) = (N_1)^{-1/2}\sum_{\mathbf{n}} e^{i2\pi k_1 n_1/N_1}$, with $k_1 = 0, \pm1, \pm2, \ldots, \pm(N_1/2-1), N_1/2$ for N_1 even ($k_1 = 0, \pm1, \pm2, \ldots, \pm(N_1-1)/2$ for N_1 odd). Of course, assuming periodic boundary conditions is only reasonable in the limit of large N_1. In particular, for the calculation of the circular dichroism spectrum, these boundary conditions turn out only to give reliable results for very long cylinders (hundreds of rings), as will be illustrated in the next section [6].

In view of these strong restrictions on using periodic boundary conditions, we have recently also explored another approach for obtaining analytical solutions to the longitudinal wave functions, which does account for the finite length of the cylinder with the appropriate open boundary conditions. This approach is rooted in a previous study of Malyshev and Moreno [9], who argued that simple standing sine waves are good approximations for the exciton wave functions of a chain with long-range point–dipole interactions. Using this idea, we have shown [7] that in the $k_2 = 0$ band, the wave functions

$$\varphi_{k_1}(n_1;k_2=0) = \sqrt{\frac{2}{N_1+1}} \sin\frac{\pi k_1 n_1}{N_1+1} \quad (4)$$

($k_1 = 1, 2, \ldots, N_1$), which are exact for interactions between nearest-neighbor rings in the aggregates, are good approximations to the exact wave functions if the cylinder is not too short (in practice, in the order of 100 rings or longer for aggregates of the structure of chlorosomes of green bacteria). This was shown by direct comparison of the ansatz Eq. (4) to the numerically calculated exact wave functions. In addition, we showed the validity of this approximation by calculating the ratio of the mixing matrix elements of the actual long-range interactions between different k_1 states to the difference of the diagonal matrix elements of

these interactions in both states involved. We showed that generally this ratio is small ($\leqslant 0.1$ for $N_1 > 50$ for cylinders of the chlorosome structure), and moreover, independent of the cylinder structure, this ratio decreases logarithmically for growing N_1.

For the $k_2 = 1$ band, we used an analogous ansatz [7]:

$$\varphi_{k_1}(n_1; k_2 = 1) = \sqrt{\frac{2}{N_1 + 1}} e^{i(\theta+\gamma)n_1} \sin \frac{\pi k_1 n_1}{N_1 + 1}, \tag{5}$$

where $\theta + \gamma$ accounts for the complex nature of the effective Hamiltonian for $k_2 = 1$. If effective interactions would only occur between neighboring rings, Eq. (5) would be exact, with $\theta + \gamma$ the argument of the complex nearest-neighbor interaction. It turns out that in the presence of long-range interactions, θ can be obtained from an optimization condition that guarantees that the mixing between states of the type Eq. (5) induced by the actual long-range interactions does not diverge for long cylinders. For cylinders (of the chlorosome structure) longer than roughly 100 rings, the thus obtained states compare well to numerically obtained exact ones, and show an interesting chiral behavior of the excitation density on the cylinder's surface as a consequence of the fact that $\theta \neq 0$ [7].

4. Linear optical spectra

The general expressions for the absorption spectrum $A(\omega)$ and the linear and circular dichroism spectra (LD(ω) and CD(ω), respectively), may be derived using the Fermi golden rule and can be found in Ref. [6]. For homogeneous aggregates the symmetry of the system quite generally dictates that only in the $k_2 = 0$ and the $k_2 = \pm 1$ bands states occur that contribute to these spectra (selection rules). The states in the $k_2 = 0$ band have a transition dipole parallel to the cylinder's axis, while those in the $k_2 = \pm 1$ bands are polarized perpendicular to this axis. In practice, in each of these bands only a few states have strong absorption oscillator strengths. In particular, in the limit of long cylinders, using periodic boundary conditions in the longitudinal (N_1) direction, in each of these bands only one state with oscillator strength occurs, leading to a total of three superradiant states: $(k_1, k_2) = (0, 0)$, $(N_1\gamma/2\pi, 1)$, and $(-N_1\gamma/2\pi, -1)$ [6,10]. For shorter cylinders, using the ansätze Eqs. (4) and (5), one finds seven superradiant states [7], one in the $k_2 = 0$ band and three in the $k_2 = 1$ and the $k_2 = -1$ bands. The latter are pairwise degenerate. The superradiant states dominate the absorption and LD spectra through peaks that occur at the energies corresponding to their eigenenergies. The CD spectrum is somewhat more complicated, as it also contains dispersive (derivative) spectral features at the energies of the superradiant states.

We have used the general expressions for $A(\omega)$, LD(ω), and CD(ω) to calculate those spectra for two types of cylindrical aggregates: the chlorosomes of the green bacterium *Chloroflexus aurantiacus* [6,7] and the synthetic aggregates that are formed through self-assembly of the dye $5, 5', 6, 6'$-tetrachlorobenzimidacarbocyanine with $1, 1'$-dioctyl and $3, 3'$-bis(3-sulfopropyl) substituents (hereafter abbreviated C8S3) [11]. In the remainder of this section we will address some of the salient results.

The chlorosomes of *Chloroflexus aurantiacus* are cylindrical aggregates of BChl *c* molecules with a known structure determined by the parameters [2,12]: $R = 2.297$ nm, $N_2 = 6$, $h = 0.216$ nm, $\alpha = 189.6^\circ$ (in Ref. [12] this angle was misplaced by its complement [13]), $\beta = 36.7^\circ$, and $\gamma = 20^\circ$. Furthermore, we have taken ω_0 to agree with a single-molecule absorption peak at 675 nm and we have used $\mu^2 = 20D^2$ for the square of the single-molecule transition dipole. Using these parameters and taking into account all dipole-dipole interactions within the cylinder, we have performed exact diagonalizations of the $k_2 = 0$ and the $k_2 = 1$ bands and used the results to obtain the exact spectra $A(\omega)$, LD(ω), and CD(ω). In addition, we have calculated these spectra using the two analytical approaches described in Section 3 to obtain the exciton eigenfunctions.

Fig. 2 shows the results for chlorosomes of length $N_1 = 75$, 150, and 400. The solid curves represent the exact spectra, the dotted curves were obtained using periodic boundary conditions in

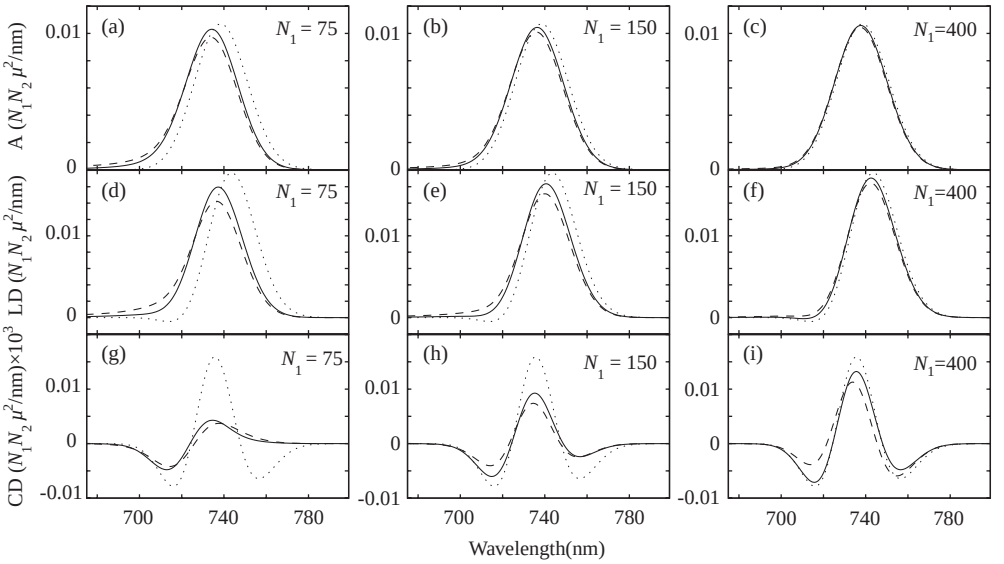

Fig. 2. Absorption spectra (a)–(c), linear dichroism spectra (d)–(f), and circular dichroism spectra (g)–(i) for cylinders of the chlorosome structure with three different lengths N_1. Solid, dotted, and dashed curves represent the results as obtained, respectively, from exact numerical diagonalization, from periodic boundary conditions, and from our ansatz wave functions (Eqs. (4) and (5)).

the N_1 direction (in the infinite-length limit), while the dashed curves have been obtained using the ansätze Eqs. (4) and (5). The linewidth of the spectral peaks was generated by convoluting the exciton stick spectra with a Gaussian lineshape function of full width at half maximum $W = 500\,\mathrm{cm}^{-1}$. It is clear from the figure that for the cylinder length considered, the results obtained using the ansatz wave functions give a very good description of the exact spectra. Apparently, the ansätze properly account for the finite-size effects. By contrast, we observe that if we use periodic boundary conditions only the absorption and the LD spectrum are well described, while the CD spectrum at smaller values of N_1 even qualitatively deviates from the exact result. This illustrates the fact that the CD spectrum very slowly converges towards the infinite-length spectrum.

The sensitivity of the CD spectrum to the cylinder length, illustrated by Fig. 2, is interesting in its own right and has been studied by us in greater detail in Ref. [6], as well as by Prokhorenko et al. [14]. We have found that the absorption and LD spectrum quickly converge towards their infinite-length shapes and hardly change shape for N_1 larger than 50. By contrast, the shape of the CD spectrum even for $N_1 > 50$ still undergoes large qualitative changes. This sensitivity to N_1 originates from the fact that the CD spectrum contains close lying positive and negative features whose exact positions are very sensitive to N_1. Thus, the overall shape of the spectrum, which results from the subtle balance between the positive and negative features, is strongly influenced by small changes in N_1 [6].

The strong variation of the CD with the cylinder length offers an explanation to a well-known problem in the literature on chlorosomes, namely the strong variation of this spectrum as observed in different experiments [15–20]. Two types of spectra are typically reported in the experimental literature. The first has a high-wavelength positive peak and a low-wavelength negative dip, much like our exact spectrum in Fig. 2(g), while the second type has a positive peak, surrounded by two dips, like in Fig. 2(h,i). It is important to note that the qualitative changes in the CD spectrum observed around $N_1 = 100$ are not accompanied by any noticeable changes in the absorption and LD spectra. Indeed, the big differences observed in the

CD spectra reported from different experiments, are accompanied by only very minor changes in the absorption and LD spectra. These results lead us to conjecture that the differences in the reported experimental results originate from the fact that different sample preparation and handling routines lead to chlorosomes of different length [6,14]. Electromicrographes lend further support to this conclusion [20].

We now turn to the tubular C8S3 aggregates. Using cryo-TEM [11], it has been established that these are double-wall cylinders, consisting of two concentric tubes of diameters 11 and 16 nm, respectively. The hydrophobic sidegroups of the dye molecules fill the space between both cylinders, while the hydrophilic groups extend into the solvent. The cryo-TEM technique lacks the resolution to determine the molecular packing in each of the cylindrical surfaces. The absorption and LD spectra for these aggregates reveal three exciton bands [11]. The two lowest-energy ones of these (at 602 and at 592 nm) are polarized along the tube's axis, while the highest-energy one (at 580 nm) is polarized perpendicular to this axis. These features may be explained using the simple notion of three superradiant states per cylinder, as predicted when using periodic boundary conditions in the N_1 direction. As two of these transitions are degenerate, this leads to two absorption peaks, with mutually perpendicular polarization directions. The observed spectra for C8S3 tubes may then be explained by assuming that the separation between the transitions perpendicular to the tube's axis for inner and outer cylinders have a spectral separation that is smaller than the linewidth, thus leading to one effective absorption peak at 580 nm.

Indeed, it may be shown that a model of two weakly interacting concentric cylinders, formed by consistently wrapping bricklayer monolayers on cylindrical surfaces of appropriate diameter, gives good fits to the observed spectra [11]. Here the fit parameters are the lattice shift of adjacent molecular rows in the bricklayer structure and the angle that determines the direction in which the monolayer is rolled. It should be noted that including the effects of energetic disorder improves the quality of the fit [11]. However, the salient features of the spectrum can be well understood already within a completely homogeneous model.

5. Concluding remarks

We have presented a brief overview of recent research on excitons and the related optical properties in molecular aggregates with a tubular shape. A homogeneous Frenkel exciton model gives a good description of the most salient optical properties that have been observed for such aggregates. In particular, this model explains the experimentally observed large variation in the CD spectra of chlorosomes. Also the polarization-dependent spectra of double-wall C8S3 nanotubes may be understood from this basic model. Inclusion of energetic disorder in general improves the agreement between theory and experiment, but it is striking that the essential spectral features can be well understood in terms of a completely homogeneous model. The special localization properties of excitons in disordered cylindrical aggregates are analyzed in Ref. [21].

In this paper, we only addressed the linear optical response. Nonlinear experiments, in particular pump–probe spectroscopy, has also been used to study tubular aggregates [22]. The pump–probe spectra of tubular J aggregates are very similar in nature to those of linear aggregates, which may be explained from an effective Pauli exclusion for excitons to reside on the same ring [23]. Further studies into time-resolved pump–probe spectra and the interpretation in terms of exciton transport [24] are topics of current interest.

Acknowledgements

It is a pleasure to thank Prof. Vladimir M. Agranovich for his constant interest in our work on molecular aggregates. This work is part of the research program of the Stichting voor Fundamenteel Onderzoek der Materie (FOM), which is financially supported by the Nederlandse Organisatie voor Wetenschappelijk Onderzoek (NWO).

References

[1] L.A. Staehelin, J.R. Golecki, G. Drews, Biochim. Biophys. Acta 589 (1980) 30.
[2] A.R. Holzwarth, K. Schaffner, Photosynth. Res. 41 (1994) 225.
[3] S. Kirstein, H. von Berlepsch, C. Böttcher, C. Burger, A. Ouart, G. Reck, S. Daehne, Chem. Phys. Chem. 3 (2000) 146.
[4] A. Pawlik, A. Ouart, S. Kirstein, H.-W. Abraham, S. Dähne, Eur. J. Org. Chem. (2003) 3065.
[5] C. Spitz, J. Knoester, A. Ouart, S. Daehne, Chem. Phys. 275 (2002) 271.
[6] C. Didraga, J.A. Klugkist, J. Knoester, J. Phys. Chem. B 106 (2002) 11474.
[7] C. Didraga, J. Knoester, J. Chem. Phys, 121 (2004) 946.
[8] V.M. Agranovich, Zh. Exp. Teor. Fiz. 37 (1959) 430 [Engl. transl. Sov. Phys. JETP 37 (1960) 307];
V.M. Agranovich, Fiz. Tverd. Tela 3 (1961) 811 [Engl. transl. Sov. Phys. Solid State 3 (1961) 592].
[9] V. Malyshev, P. Moreno, Phys. Rev. B 51 (1995) 14587.
[10] O.J.G. Somsen, R. van Grondelle, H. van Amerongen, Biophys. J. 71 (1996) 1934.
[11] C. Didraga, A. Pugžlys, P.R. Hania, H. von Berlepsch, K. Duppen, J. Knoester, J. Phys. Chem. B, in press.
[12] V.I. Prokhorenko, D.B. Steensgaard, A.R. Holzwarth, Biophys. J. 79 (2000) 2105.
[13] V.I. Prokhorenko, private communication.
[14] V.I. Prokhorenko, D.B. Steensgaard, A.R. Holzwarth, Biophys. J. 85 (2003) 3173.
[15] R.J. van Dorssen, H. Vasmel, J. Amesz, Photosynth. Res. 9 (1986) 33.
[16] R. Frese, U. Oberheide, I. van Stokkum, R. van Grondelle, M. Foidl, J. Oelze, H. van Amerongen, Photosynth. Res. 54 (1997) 115.
[17] K. Griebenow, A.R. Holzwarth, F. van Mourik, R. van Grondelle, Biochim. Biophys. Acta 1058 (1991) 194.
[18] B.D. Steensgaard, C.A. van Walree, H. Permentier, L. Bañeras, C.M. Borrego, J. Garcia-Gil, T.J. Aartsma, J. Amesz, A.R. Holzwarth, Biochim. Biophys. Acta 1457 (2000) 71.
[19] J.M. Olson, P.D. Gerola, G.H. van Brakel, Springer Ser. Chem. Phys. 42 (1985) 67.
[20] R.P. Lehmann, R.A. Brunisholz, H. Zuber, Photosynth. Res. 41 (1994) 165.
[21] C. Didraga, J. Knoester, J. Chem. Phys, in press.
[22] S.S. Lampoura, C. Spitz, S. Daehne, J. Knoester, K. Duppen, J. Phys. Chem. B 106 (2002) 3103.
[23] M. Bednarz, J. Knoester, J. Phys. Chem. B 105 (2001) 12913.
[24] P. Reineker, C. Warns, C. Supritz, I. Barvík, J. Lumin. 102–103 (2003) 802.